Composites Science and Technology, Volume 128, 18 May 2016, Pages 138-146
DOI:10.1016/j.compscitech.2016.03.019

On the self-sensing functions of CFRP Z-pins and reinforced composite laminates

B. Zhang[a,*], G. Allegri[b], M. Yasaee[a], S.R. Hallett[a], I.K. Partridge[a]

[a]Advanced Composites Centre for Innovation and Science (ACCIS),

University of Bristol, Queen's Building, University Walk, Bristol BS8 1TR, UK

[b] Department of Aeronautics, Imperial College London,

South Kensington Campus, London SW7 2AZ, UK

Abstract

This paper for the first time validates the self-sensing function of Z-pin reinforced composite laminates. T300/BMI Z-pins are considered in this study. The self-sensing performance of the CFRP rod is first evaluated under tension, with the electrical resistance (ER) along the Z-pin length measured as the sensing variable. Experiment results show that a carbon-fibre Z-pin is an excellent self-sensor under tensile loading. The ER gauge factor is constant up to 0.8% elongation, and then it increases gradually until the Z-pin ruptures. The self-sensing function of single CFRP Z-pin reinforced laminates is then evaluated under Mode I and Mode II bridging loading. The laminate through-thickness ER (TTER) is measured via surface electrodes attached to the protruding ends of a Z-pin. If the through-thickness reinforced laminate is electrically conductive, the whole Z-pin pull-out process can be monitored. However, for a non-conductive laminate, delamination bridging may not be sensed after the Z-pin is pulled out from one of the surface electrodes. Regardless of the electrical property of the reinforced laminate, the ER is capable of detecting Mode II bridging, albeit there exists an initial "blind spot" at relatively small lateral deformation. However, the Z-pin rupture can be clearly detected as an abrupt ER increase. This study paves the way for exploring multi-functional applications of through-thickness reinforcement.

Keywords: A. Structural composites; A. Smart materials; B. Delamination; Z-pinning

*Corresponding author: b.zhang@bristol.ac.uk (B. Zhang); +44(0) 117 33 15311

1. Introduction

Multi-functional composites have seen increased interest over the past two decades, as in comparison with traditional composites they can provide non-load-bearing functions, such as sensing, actuation and energy harvesting [1]. Multi-functional composites can be classified into two categories based on the functioning source: additional-phase activated composites and self-functioning composites. A typical additional-phase activated composite is the carbon-nanotube-filled composite, which have been proven to present sensing and actuating functions [2,3]. A carbon-fibre reinforced polymer (CFRP) can be regarded as a self-functioning composite, as it offers a delamination self-sensing function via ER or electric potential measurements [4–6].

Traditional polymer-based composite laminates possess excellent in-plane performance, but they are prone to suffer delamination between plies, particularly when subjected to impact. Thus several through-thickness reinforcement (TTR) technologies such as stitching, 3D weaving and tufting have been developed to improve interlaminar strength and toughness of composite laminates [7]. Z-pinning is an effective TTR technology, whereby small diameter rods (Z-pins) are inserted through the thickness of laminates [8]. The mechanical performance of Z-pinned composites has been assessed in several experimental [9,10] and modelling studies [11–13]. However, the multi-functionality of Z-pinned composites has not been investigated in the open literature yet, although a conceptual investigation of the sensing performance of piezoelectric Z-pin reinforced laminates has been proposed in [14]. The most commonly used Z-pin can be denoted as a small-scale CFRP rod, since it is reinforced by carbon-fibre strands and consolidated by BMI [15]. A small scale CFRP rod has been shown to possess a strain sensing function via ER measurement [16]. Z-pins can be in principle made of any material that can be processed into thin rods. It means that the self-sensing function of Z-

pinned laminates may be enabled by TTR elements. Therefore, it is worth exploring the sensing behaviour of through-thickness reinforced composites. In this study we consider 0.28 mm diameter T300/BMI Z-pins, which have 1 k filament count tows and a fibre volume fraction of approximately 0.57.

This paper for the first time validates the self-sensing function of Z-pin reinforced laminates. This project evaluates first the sensing function of a CFRP rod under tension, and then the sensing performance of single CFRP Z-pin reinforced laminates under Mode I and Mode II bridging loading. The ER along the Z-pin length is measured to sense the longitudinal strain in tension tests. For the bridging tests, the laminate through-thickness conductivity is measured via surface electrodes attached to the protruding ends of a Z-pin. This paper concludes with a discussion on multi-functionality aspects of the TTR elements and reinforced laminates.

2. Specimen preparation

Fig. 1 shows the configuration of single Z-pin tension coupons, which have 20 mm gauge length. The mechanical loading was applied via two glass-fibre reinforced polymer (GFRP) tabs, which were bonded to the pin using AS89.1/AW89.1 adhesive (Cristex Ltd, UK). The bonding length equals to 25 mm on each side. The tabs were aligned to the Z-pin using a paper card [17]. Two outer electrodes and two inner electrodes were bonded to the Z-pin ends, for current injection and voltage measurement respectively. Thus a 4-wire ER measurement set-up was employed in order to factor out the effect of Z-pin/electrode contact ER. Silver/epoxy conductive adhesives (1:1 weight ratio) were used for manufacturing the electrodes. The electrodes were cured at 80 °C for 15 minutes in an oven. The electrodes were positioned outside of the gauge length, in order to avoid damaging the Z-pin/electrode interfaces while applying the mechanical load. Each electrode was also bonded to a conductive wire.

As shown in Fig. 2a, the coupon configuration for single Z-pin bridging tests is analogous to that tested in [9], but some modifications were introduced in order to accommodate the electrodes. The coupon consists of a prismatic laminate block, which is split into two halves on the mid-plane by a PTFE release film. The laminate was made of 48 plies of unidirectional prepreg, with a stacking sequence of $[(-45/90/45/0)_s]_6$. Two different prepreg materials were employed, namely: conductive IM7/8552 prepreg; and non-conductive E-glass/913 prepreg (Hexcel, UK). The average thickness is 6.0 mm for the CFRP laminate, while it is 6.8 mm for the GFRP laminate. A single Z-pin was inserted through the thickness of the laminate, with 1 mm length protruding from the top and bottom surfaces of the laminate. Two prismatic electrodes were bonded to the protruding Z-pin ends for ER measurement. Thus, a 2-wire ER measurement method was used in the bridging test. Each electrode had 5×5 mm^2 in-plane dimensions. The same electrode material was used for both the bridging and tensile coupons. For sake of clarity, a CFRP TTR rod connected to the electrodes is called a "sensing" Z-pin; otherwise one shall refer to the TTR rod as a "mechanical" Z-pin.

Due to the electrode arrangement, the single sensing Z-pin bridging coupon requires a different manufacture process in comparison with a single mechanical Z-pin specimen described in [9]. More in detail, 1 mm thick rubber sheets were placed on the bottom and top surfaces of the laminates. The Z-pins were inserted through the entire thickness of the laminate/rubber sheets assembly, as shown in Fig. 2b. The Z-pin ends were then sheared off on the rubber sheets. The plate was then cured in an autoclave following the manufacturer's recommendations (2 h at 180 °C and 100 psi for CFRP laminate, 1 h at 125 °C and 100 psi for GFRP laminate). The rubber sheets were peeled off after cure, leaving 1 mm long Z-pin ends protruding from two sides. Next, the plate was carefully cut into individual coupons, as shown in Fig. 2c. The surfaces of the coupons were

cleaned by acetone before bonding the electrodes. The latter were placed on the coupon surfaces with the aid of removable moulds, as shown in Fig. 2d. Each of moulds had a central hollow slot to accommodate and shape the electrode, as well as a side slot to hold the conductive wire in position. The electrodes were cured at 80 °C for 15 minutes in an oven, then the final single bridging coupon, shown in Fig. 2a was obtained. Note that, in the bridging coupon, the Z-pin ends were fully embedded within the electrodes.

3. Experimental set-up

All the tests were carried out via a calibrated Instron 8872 servo-hydraulic machine, equipped with a 1 kN load cell. For the tensile tests, the coupons were gripped at the end tabs, as shown in Fig. 3. The tensile load was applied at the rate of 0.1 mm/min. The paper card attached to the specimen for alignment was carefully cut into two halves along its central line prior to testing, as indicated in Fig. 3.

As shown in Fig. 4a, Mode I loading was applied to the bridging coupons via two steel tabs. Between the specimen and each of the tabs were inserted two spacers, in order to protect the electrodes embedding the Z-pin ends. The spacers need to be electrically insulating, to eliminate any spurious effect on the measured ER. The spacers should also have high stiffness, in order to reduce the overall compliance of the loading system. In this study, each spacer was made of E-glass/913 laminate with $20 \times 4 \times 3$ mm^3 (length × width × thickness) dimensions. The spacers were bonded to the coupon and tabs using cyanoacrylate superglue (Loctite Corp., UK).

As shown in Fig. 4b, Mode II loading was applied to a bridging specimen via a modified Arcan rig, as in [9]. The central plate of the rig can be rotated to obtain various mode mixities, albeit only a 90° orientation (Mode II) was used in this study. The plate comprises a central slot to accommodate the specimen. The testing coupon was attached to the top and bottom halves of the plate using two screw clamps. This allows inserting

electrically insulating PVC tape between the coupon and the jig. As shown in Fig. 4c, each half of the plate also comprises a radially-oriented slot, which was designed to accommodate the electrodes and the wires connecting the specimen to the signal acquisition system. The Mode I and Mode II loads were both applied at a displacement rate of 0.5 mm/min. The ER signal was measured by a Keithley 2700 digital multimeter with the resolution and sample rate at 6.5 digits and 20 readings/s respectively.

4. Results and discussions

4.1 Tension tests

The results of three tension test specimens are presented in Figs. 5a-b. All the coupons exhibited a consistent mechanical response. The stress increases linearly with the tension strain, until catastrophic failure of the Z-pin. The failure strength and strain are respectively 2021 MPa and 1.5%; all the Z-pins failed in the gauge region. The results agree well with that reported in [18]. ASTM D3039 tests on unidirectional T300-12k carbon epoxy give a tensile strength of 1860 MPa [12]. The stressed volume for ASTM D3039 coupons is 2250 mm^3, while it is only 1.23 mm^3 for the tensile specimens considered here. Applying Weibull theory to predict the size effect on the strength of tensile coupons, with a Weibull modulus of 27 [12], yields a failure stress of 2456 MPa for the tensile coupons that we tested. This value is 20% higher than that experimentally obtained, but not unreasonably far off considering the difference in filament count as well as in resin system (BMI instead of epoxy). These considerations support the validity of the tensile tests presented here. In addition, it is worth noticing that Cartié et al. reported a tensile strength of only 1200 MPa for 0.51 mm CFRP Z-pins [10]. It is expected that the quality of the Z-pins used in this study has been improved, especially for the larger diameter TTR elements it becomes more difficult to consolidate.

Fig. 5b shows the sensing behaviour of the Z-pin subjected to tensile loading. The

initial ER values (R_0) of the three coupons are respectively 76.1 Ω, 67.0 Ω and 83.3 Ω. All the coupons also present a consistent trend regarding the ER variation. The ER first increases linearly up to a strain value of around 0.8%, labelled by a plus sign in Fig. 5b. Clearly this is due to elastic deformation of the Z-pin. With further loading, the ER increases at a faster rate until the complete pin failure. This can be attributed to progressive random fibre breakage within the Z-pin [16], whose onset takes place at 50% of the macroscopic failure load. The ER gauge factors for the tested coupons have consistent values up to a strain of 0.8%, for which $\Delta R/R_0 = 0.035$. On the other hand, above 0.8% strain there is quite a significant variation of gauge factor values from coupon to coupon. In order to explain this variation, it must be considered that the contacts between adjacent fibres are randomly distributed throughout the whole gauge region of a Z-pin. This randomness is further promoted when fibre failure occurs, i.e. in the strain range where the gauge factors become nonlinear.

4.2 Bridging tests

Eight bridging coupons were tested for each laminate material, namely carbon and glass. Four of the coupons were characterised under Mode I loading, while the remaining four were tested in Mode II.

4.2.1 Z-pin reinforced CFRP laminates

The typical Mode I response for a single sensing Z-pin reinforced CFRP laminate is shown in Fig. 6a. The overall Z-pin pull-out process comprises three stages: pre-debonding from electrode (stage I), pull-out from electrode (stage II) and pull-out from laminate (stage III). For sake of clarity, we will consider debonding and pull-out always starting from and initially progressing within the “top” electrode. During stage I the bridging force increases linearly with the pin elastic elongation, as shown in the zoomed view in Fig. 6b. Due to the quasi-isotropic stacking sequence of the coupon, the

Z-pin/laminate interface is severely weakened after the post-cure cool down [9,13]. Thus, the bridging force during stage I is mainly due to the Z-pin/electrode bonding and the Z-pin/laminate friction. The load peak that occurs at a small value of the applied displacement corresponds to the onset of debonding from the top electrode. This dis-bond suddenly develops and the consequent load drop is also accompanied by a shortening of the Z-pin. Regarding the TTER signal during stage I, part of the injected current flows from the top to the bottom electrode, crossing the Z-pin/electrode interfaces and travelling along the Z-pin, as illustrated by a red dashed curve in Fig. 7a. Since the CFRP laminate is conductive, part of the current also flows through the laminate thickness, crossing the Z-pin/laminate interfaces and eventually reconnecting with the Z-pin, as shown by red solid curves in Fig. 7a. According to the classic resistance parallel theory, R_T, representing the total ER associated with the top half of the coupon, can be estimated by:

$$R_T \sim (R_{TEd\_Pin} + R_{TPin}) \,//\, (R_{TEd\_TLm} + R_{TLm} + R_{TLm\_Pin}) \quad (1)$$

where "//" is the resistance parallel symbol, R_{TEd_Pin} the contact ER between the top electrode and the Z-pin, R_{TPin} the longitudinal ER of the top half Z-pin, whose value can be estimated from the tension test results, in combination with the bridging force, R_{TEd_TLm} the contact ER between the top electrode and the top sub-laminate, which is assumed to keep constant with loading. R_{TLm} is the ER of the current flowed segment of the top sub-laminate, R_{TLm_Pin} the contact ER between the top sub-laminate and the Z-pin. Thus, the two terms on the left side of the symbol indicate the equivalent ER associated with the current path indicated by the dashed curve on the top half coupon in Fig. 7a, while the terms on the right side represent the equivalent ER of the other path. The bottom half of the coupon exhibits the same ER network as the top half, thus the changing trend of the TTER can be determined based on analysis on the top half.

The TTER signal in stage I follows the traction trend, increasing until the peak load

and decreasing suddenly with the Z-pin/electrode debonding. The mechanisms causing the increasing trend include: 1) the increase of the R_{TPin} term in Eq. 1 due to the Z-pin elongation; 2) the increase of R_{TEd_Pin} due to the reduction of the Z-pin/electrode contact area, which is caused by the cross-sectional contraction of the Z-pin due to the Poisson effect and progressive failure of the Z-pin/electrode interface; (3) the increase of R_{TLm_Pin}, due to the reduction of the Z-pin/laminate contact area, which is also a result of the cross-sectional contraction of the Z-pin. For the same reason, the TTER decrease with the Z-pin/electrode debonding is because the decrease in R_{TPin} due to the Z-pin shortening, as well as in R_{TEd_Pin} and R_{TLm_Pin} due to the Poisson effect caused radial pin expansion. Comparison between Fig. 6b and Fig. 5b reveals that the fractional TTER increase in stage I of the bridging coupon is much larger than in a tension coupon. This is because the TTER change is attributed to the aforementioned three mechanisms, while only the first mechanism, i.e. the Z-pin elongation appears in the tension coupon.

In stage II, the Z-pin starts to slide within the top electrode and the top sub-laminate, as illustrated in Fig. 7b. The bridging force shows a stable increasing trend with the sliding, as shown in Fig. 6b. This is due to the presence of two enhanced friction zones (i.e. snubbing [11]), located at the ends of the Z-pin/top-laminate interface, as indicated in Fig. 7b. The enhanced friction located near the fracture surface is caused by Z-pin misalignment [9,13]. The enhanced region close to top electrode is due to the dragging of the protruding Z-pin end into the laminate. Part of electrode material is squeezed in between the Z-pin and the laminate, locally increasing the friction. This will be confirmed in the next subsection. Further increasing the bridging force, the Z-pin tends to stay bonded to the bottom electrode. The bridging force reaches its peak when full pull-out from the top electrode is achieved, as for the coupons considered in Fig. 6. On the other hand, if the friction enhancement in the top sub-laminate is large enough, the Z-pin may

also de-bond from the bottom electrode. The second debonding is marked by another load drop, as observed in a coupon whose response is shown in Fig. 8. For this case, with further loading the Z-pin is gradually pulled out from the bottom electrode, with its top end stuck within the top electrode, as illustrated in Fig. 7c. The traction still exhibits an increasing trend, due to the two additional enhanced friction zones associated with the bottom half of the Z-pin. The bridging force reaches a second peak at the point when the Z-pin is fully pulled out from the bottom electrode. The different bridging mechanisms occurring in stage II are ultimately attributed to the coupon asymmetry relative to the fracture surface. The current paths in stage II are the same as in stage I, but the TTER signal during stage II becomes nosier due to the unstable Z-pin/electrode and Z-pin/laminate contact ERs. However, the overall TTER trend follows that of the load. In the case where debonding takes place only in one electrode, the TTER tends to increase during the whole stage II, as shown in Fig. 6b. This is simply because the Z-pin/electrode interface area decreases with progressive pull-out, and thus increases the R_{TEd_Pin} term in Eq. 1. If debonding occurs in both electrodes, the TTER increases when the Z-pin slides within the top electrode. Then there is an ER drop corresponding to the second debonding, followed by a second ER increase caused by sliding within the bottom electrode, as shown in Fig. 8. The TTER changing trend associated with the debonding from the bottom electrode can be explained using the same mechanisms as for the debonding from the top electrode.

Stage III begins when the Z-pin is completely pulled out from one of the electrodes. The bridging force steadily decreases until complete pull-out from one of the sub-laminates, as shown in Fig. 6a and Fig. 8. The current path for stage III differs from those characterising stages I and II and it is illustrated in Fig. 7d and Fig. 7e for pull-out from the top sub-laminate (POFTL) and pull-out from the bottom sub-laminate (POFBL)

respectively. The difference arises because the current path, bridged by the electrodes, the Z-pin/electrode interfaces and the Z-pin, disappears in the "pull-out" half of the coupon. For the POFTL case, the R_T value can be estimated by:

$$R_T \sim R_{TEd\_TLm} + R_{TLm} + R_{TLm\_Pin} \quad (2)$$

The onset of stage III is always marked by an abrupt TTER increase. This can be easily derived by comparing Eq. 1 and Eq. 2. With further sliding, the current has to travel a longer distance through the laminate thickness before being able to reconnect with the Z-pin. This increases the R_{TLm} and R_{TLm_Pin} terms in Eq. 2, thus the TTER shows an overall increasing trend. However, the TTER is affected by noise, due to the variability in the Z-pin/laminate contact ER that is further promoted by the progressive sliding. The above analysis also applies to the POFBL case.

As shown in Fig. 9, akin to a "mechanical" Z-pin [9], the Mode II bridging force provided by a sensing Z-pin also increases monotonically with the Z-pin deformation, until a catastrophic pin rupture occurs at relatively small sliding displacements. Regarding the TTER sensing, the current path in Mode II is the same as in stage I of Mode I. The Mode II TTER signal shows no clear trend for sliding displacements less than half the Z-pin diameter. Two opposite mechanisms are responsible for this behaviour. First of all, the Z-pin experiences an increasing lateral pressure due to the shear deformation. This will increase the effective Z-pin/electrode contact area through closing some of the voids existing in the interface, thus cause an increase in conductivity between the Z-pin tips and the electrodes, i.e. decrease of the R_{TEd_Pin} term in Eq. 1. In addition, the increasing lateral pressure will also increase conductivity between adjacent fibres due to current percolation, thus decrease the R_{TPin} term in Eq. 1. Hence the lateral pressure in Mode II decreases the TTER. On the other hand, the deformation causes an axial stretching of the Z-pin, which increases the R_{TPin} term in Eq. 1. When the deformation exceeds half the Z-pin diameter,

the TTER exhibits a steadily increasing trend. This is due to the progressive fibre failure that takes place within Z-pin segment close to the fracture plane [9,12,13]. The TTER becomes very large when the Z-pin has fully failed. Hence, the gauge factor shown in Fig. 9 appears to diverge.

4.2.2 Z-pin reinforced GFRP laminates

The CFRP Z-pin provides the same delamination bridging mechanism when inserted either in GFRP or CFRP laminates. This is true for Mode I and Mode II loading. However, only the current paths indicated by red dashed curves in Fig. 7 exist in the GFRP coupon, since the GFRP laminate is non-conductive. Thus, the R_T of the GFRP coupon in stages I and II can be estimated by:

$$R_T \sim R_{TEd\_Pin} + R_{TPin} \tag{3}$$

As shown in Fig. 10b and Fig. 10d, the Mode I TTER shows sensing ability in stage I when inserted in a non-conductive laminate. The initial delamination loading can be sensed as linear TTER increase, and the Z-pin/top-electrode debonding can be detected by an apparent TTER drop. The TTER increase is attributed to the R_{TPin} increase due to the Z-pin elongation, and the R_{TEd_Pin} increase due to the reduction of the Z-pin/electrode contact area. It is worth observing that the fractional TTER increase at stage I in the non-conductive laminate is one order of magnitude less than in the conductive laminate. This is because different current paths exist in the two coupons. Further comparing Eq. 1 and Eq. 3, it can be found that the R_{TLm_Pin} increase at stage I in the CFRP laminate coupon may be the main reason for the amplitude difference. This can be understood via an extreme case whereby R_{TLm_Pin} becomes quite large and the current paths indicated by solid lines in Fig. 7a may disappear in the CFRP coupon. This case gives the maximum fractional TTER change in the CFRP coupon, and also the maximum difference between the two coupons.

In stage II, the TTER shows no clear overall changing trend, attributed to two opposite mechanisms. The Z-pin/electrode contact ER, i.e. R_{TEd_Pin} in Eq. 1 is increased with the decrease in the Z-pin/electrode contact area. On the other hand, the enhanced-friction effect happening close to the electrode may consolidate the Z-pin/electrode contact, and thus reduce the R_{TEd_Pin}. The Z-pin/electrode debonding can be clearly detected as an abrupt ER decrease. The full pull-out from one of the electrodes can be detected by a further ER jump. In stage III, the current paths illustrated by red dashed lines in Figs. 7d-e may become broken in the pull-out half of the coupon. Hence, the TTER may become extremely large and lose sensing ability, as shown in Fig. 10a. However, quite surprisingly, the TTER signal presented in Fig. 10c reveals a sensing ability in stage III. The reason for this rather peculiar behaviour can be understood via observing the post-mortem micrograph presented in Fig. 11. One can immediately observe the presence of carbon fibres, initially belonging to the Z-pin, which remained attached to the surface of the pull-out channel. These fibres provide electrical connection between the Z-pin and the electrode even when the pin end is dragged into the non-conductive laminate. In the enlarged view of Fig. 11, one can also observe debris of the electrode material being dragged into the pull-out channel. Apart from enhancing the Z-pin/laminate friction, this also contributes to maintain electrical connection during pull-out, allowing sensing the progression of stage III. However, the resulting TTER variation is characterised by a noise level much larger than in the CFRP coupons. Finally, as shown in Fig. 12, the Mode II response of a Z-pin in a non-conductive laminate can also be monitored via ER measurement. The TTER gauge factors for the Mode II response in GFRP laminates are similar to those observed in CFRP coupons. However, the “blind region” where no significant variation in ER occurs is larger in GFRP coupons than in CFRP laminates. An increase in TTER is noticeable only for lateral displacements exceeding one Z-pin

diameter.

4.3 Discussions on multi-functionalities of CFRP Z-pins and reinforced laminates

Sections 4.1-2 demonstrate that a CFRP Z-pin is multi-functional, since they can perform a sensing unit for a strain gauge and a laminate, as well as a delamination bridging element for the latter. Regarding the "sensing" role, the CFRP Z-pin can be used to measure small tensile strains up to 0.8%. Above the aforementioned stress level, it is impossible to obtain realistic strain values. Nonetheless, incipient damage (fibre failure) within the Z-pin can still be detected from the onset of non-linearity in the ER signal. On the other hand, when inserted in a laminate the Z-pin ER is not the single factor affecting the TTER signal measured using the sensing configuration illustrated in Fig. 2a. The Z-pin/electrode contact ER, the Z-pin/laminate contact ER and the laminate conductivity all affect the TTER. Quantitative evaluation on the extent to which the Z-pin ER affect the TTER is under investigation. However, the presence of the Z-pin enables the above sensing mechanisms. The Z-pin also upgrades the TTER sensing ability of a pinned laminate to a much higher level than of an un-pinned laminate [19]. Moreover, the CFRP Z-pin endows a non-conductive laminate with a sensing function. Regarding the "mechanical" role, in comparison with a mechanical Z-pin, the sensing Z-pin is subjected to additional frictional forces provided by the Z-pin/electrode interface and the enhanced friction zones formed due to dragging protruding pin ends into the laminate. As such, the sensing Z-pin also provides a larger pull-out resistance. Referring to the parametric study of Z-pin bridging ability in [13], the pin bridging performance in Mode I dominated cases may be improved due to the presence of the electrodes. However, when approaching a Mode II dominated regime, the pin may fail at a lower lateral deformation. Overall, the presence of electrodes may induce an earlier transition from complete pull-out to Z-pin failure with respect to the mode-mixity.

Regarding the self-sensing performance of a laminate reinforced with CFRP Z-pins, the whole Mode I bridging process can be monitored via TTER. The bridging mechanisms that can be sensed include: 1) the initial delamination loading detected as a linear ER increase; 2) the Z-pin/electrode debonding, sensed as an abrupt ER drop; 3) the Z-pin pull-out from the de-bonded electrode, detected as an overall ER increase; 4) the complete pull-out from one of the electrodes, corresponding to a sudden ER jump; 5) final pull-out stage from the laminate, characterised by an ER increase. On the other hand, if the laminate is non-conductive, the TTER allows sensing the progressive development of mechanisms 1, 2 and 4. Mechanism 3 cannot be sensed in non-conductive laminates. Mechanism 5 could also be sensed in non-conductive laminates, depending on the density of the residual Z-pin fibres that remain attached to the surface of the pull-out channel. Regarding Mode II bridging, the Z-pin deformation can also be monitored by the TTER measurement, regardless of the conductivity of the laminate. However, there exists an initial "blind region" at relatively small shear deformation. The Z-pin rupture under Mode II loading is always clearly detected as an abrupt ER increase. In terms of sensing ability, it is not the absolute value of the gauge factor that counts, but its trend of variation.

5. Conclusions

This paper has investigated the sensing functions of T300/BMI Z-pins and reinforced composite laminates. These functions were characterised by measuring the Z-pin longitudinal ER under tension loading and the TTER of single Z-pin reinforced laminates. The experimental results show that a CFRP Z-pin is an excellent strain gauge, having a gauge factor that keeps almost constant up to 0.8% elongation and gradually increases under further deformation until complete breakage. A simple 2-wire TTER measurement method was designed for Z-pinned laminates. Two electrodes were attached to the pin ends protruding from top and bottom surfaces of the laminate. The TTER is capable of

sensing the whole Mode I bridging process of the Z-pin when inserted in an electrically conductive laminate. On the other hand, in a non-conductive laminate, the TTER sensing may be lost after debonding from one of the electrodes has taken place. However, the point at which the Z-pin is fully pulled out from one of the electrodes can be detected as an abrupt TTER increase. The Mode II TTER exhibits a consistent increasing trend for both the conductive and non-conductive laminates. Nonetheless, there exists an initial "blind region" for relatively small lateral deformations in the order of one Z-pin diameter or less. The Z-pin rupture can be clearly detected as a sudden TTER increase. The electromechanical characterisation of Z-pins and reinforced laminates presented in this study provides the fundamentals for the development of multi-functional through-thickness reinforced composite structures.

Acknowledgements

The authors would like to acknowledge Rolls-Royce plc for the support of this research through the Composites University Technology Centre (UTC) at the University of Bristol.

References

[1] Pinto F. Smart multifunctional composite materials for improvement of structural and non-structural properties. PhD Dissertation, University of Bath, 2013.

[2] Gallo GJ, Thostenson ET. Electrical characterization and modeling of carbon nanotube and carbon fiber self-sensing composites for enhanced sensing of microcracks. Mater Today Commun 2015;3:17–26.

[3] Li C, Thostenson ET, Chou T-W. Sensors and actuators based on carbon nanotubes and their composites: A review. Compos Sci Technol 2008;68:1227–49.

[4] Wang X, Chung DDL. Continuous carbon fibre epoxy-matrix composite as a sensor of its own strain. Smart Mater Struct 1996;5:796–800.

[5] Todoroki A, Samejima Y, Hirano Y, Matsuzaki R. Piezoresistivity of unidirectional carbon/epoxy composites for multiaxial loading. Compos Sci Technol 2009;69:1841–6.

[6] Wang S, Chung DDL, Chung JH. Impact damage of carbon fiber polymer–matrix composites, studied by electrical resistance measurement. Compos Part A Appl Sci Manuf 2005;36:1707–15.

[7] Mouritz AP. Review of z-pinned composite laminates. Compos Part A Appl Sci Manuf 2007;38:2383–97.

[8] Partridge IK, Cartié DDR. Delamination resistant laminates by Z-Fiber® pinning: Part I manufacture and fracture performance. Compos Part A Appl Sci Manuf 2005;36:55–64.

[9] Yasaee M, Lander JK, Allegri G, Hallett SR. Experimental characterisation of mixed mode traction–displacement relationships for a single carbon composite Z-pin. Compos Sci Technol 2014;94:123–31.

[10] Cartié DDR, Cox BN, Fleck NA. Mechanisms of crack bridging by composite and metallic rods. Compos Part A Appl Sci Manuf 2004;35:1325–36.

[11] Cox BN. Snubbing effects in the pullout of a fibrous rod from a laminate. Mech Adv Mater Struct 2005;12:85–98.

[12] Allegri G, Yasaee M, Partridge IK, Hallett SR. A novel model of delamination bridging via Z-pins in composite laminates. Int J Solids Struct 2014;51:3314–32.

[13] Zhang B, Allegri G, Yasaee M, Hallett SR. Micro-mechanical finite element analysis of Z-pins under mixed-mode loading. Compos Part A 2015;78:424–35.

[14] Gu B, Zhang H, Wang B, Zhang S, Feng X. Fracture toughness of laminates reinforced by piezoelectric z-pins. Theor Appl Fract Mech 2015;77:35–40.

[15] Lander JK. Designing with z-pins: locally reinforced composite structures. PhD Dissertation, Cranfield University, 2008.

[16] Okuhara Y, Matsubara H. Memorizing maximum strain in carbon-fiber-reinforced plastic composites by measuring electrical resistance under pre-tensile stress. Compos Sci Technol 2005;65:2148–55.

[17] ASTM-C1557-03. Standard Test Method for Tensile Strength and Young's Modulus of Fibers. ASTM Int 2012.

[18] Wang X, Li C. Experimental study on pull-out strength of Z-pins. J Mater Eng 2011;1:1–4.

[19] Shen L, Li J, Liaw BM, Delale F, Chung JH. Modeling and analysis of the electrical resistance measurement of carbon fiber polymer–matrix composites. Compos Sci Technol 2007;67:2513–20.

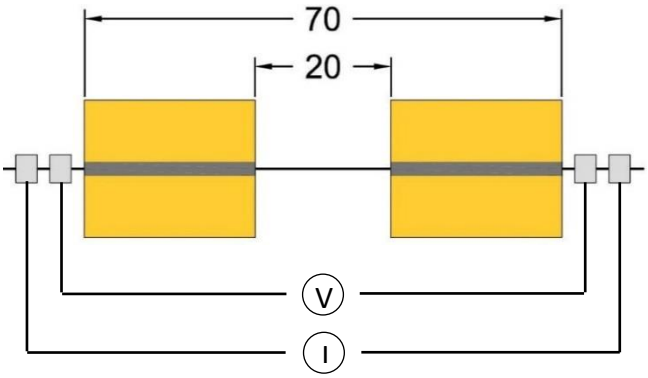

Fig. 1. Configuration of single Z-pin tensile test coupon (mm).

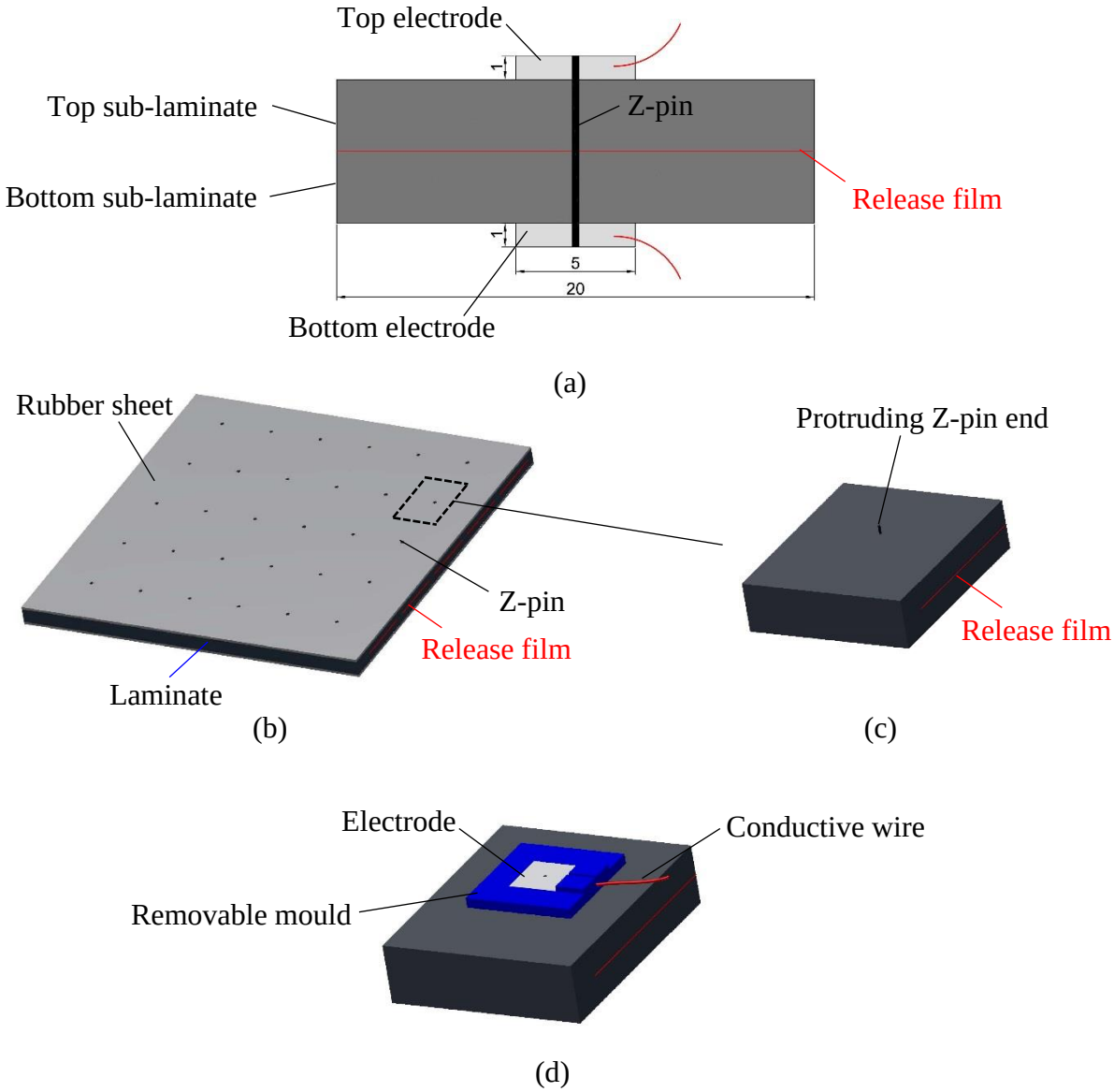

Fig. 2. (a) Single sensing Z-pin coupon for bridging test; (b) un-cured laminate plate with inserted pins and attached rubber sheets; (c) initial coupon with bare Z-pin ends; (d) electrode arrangement with the aid of removable moulds.

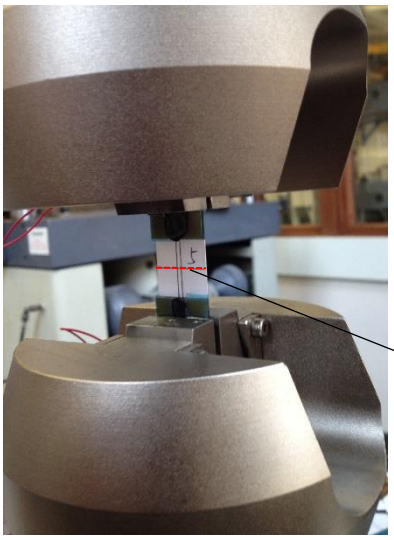

Fig. 3. Set-up for tensile loading.

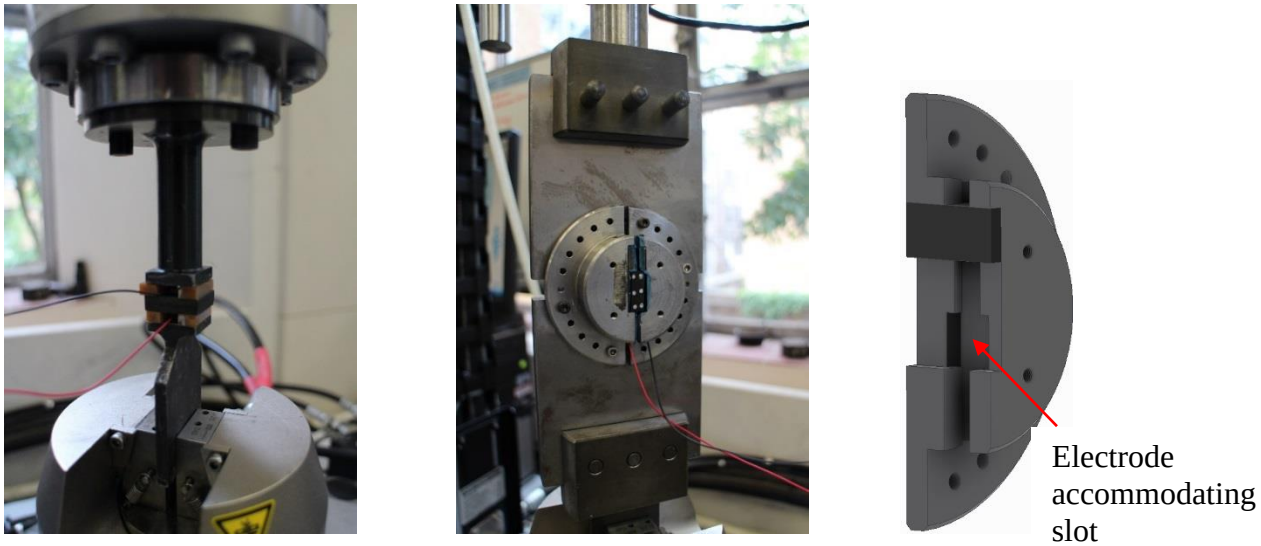

(a) (b) (c)

Fig. 4. Set-up for (a) Mode I and (b) Mode II bridging loading; (c) half of the Arcan jig.

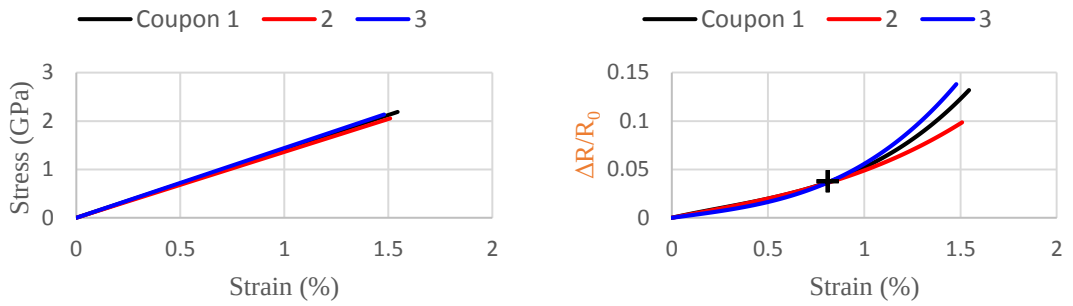

(a) (b)

Fig. 5. Tension results of three CFRP Z-pins; (a) stress and (b) fractional ER change.

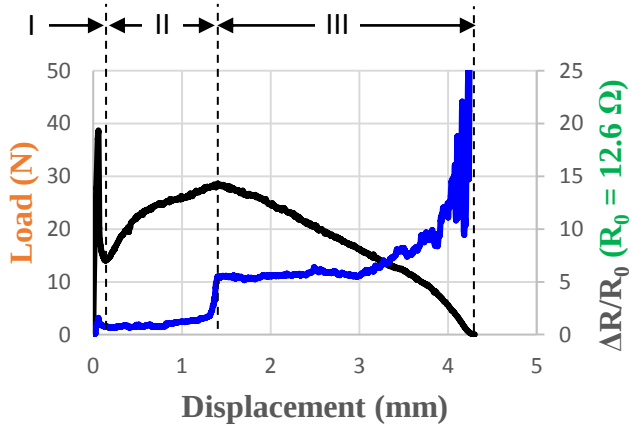

(a)

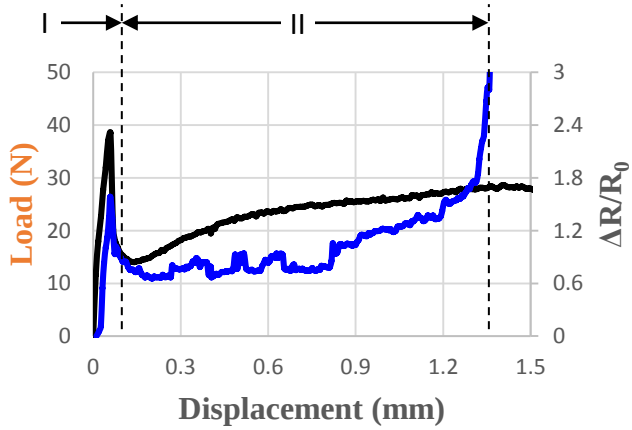

(b)

Fig. 6. (a) full-range and (b) partially enlarged plots of Mode I results of single Z-pin reinforced CFRP laminate with debonding from one electrode; black lines indicating bridging forces; blue lines showing fractional TTER changes.

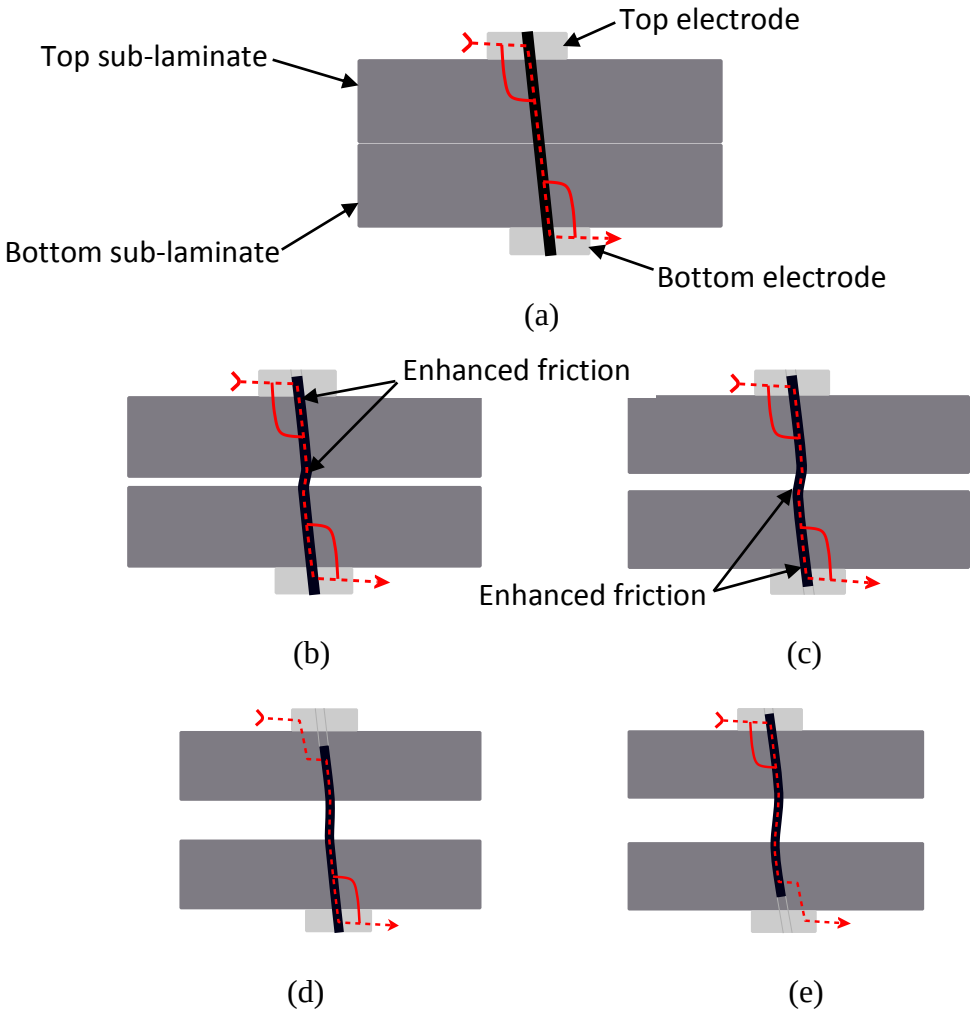

Fig. 7. Pull-out snapshots of the Z-pin with sensing configuration; (a) stage I: pre-debonding from electrode; stage II: pull-out from (b) top electrode and (c) bottom electrode; stage III: pull-out from (d) top sub-laminate and (e) bottom sub-laminate.

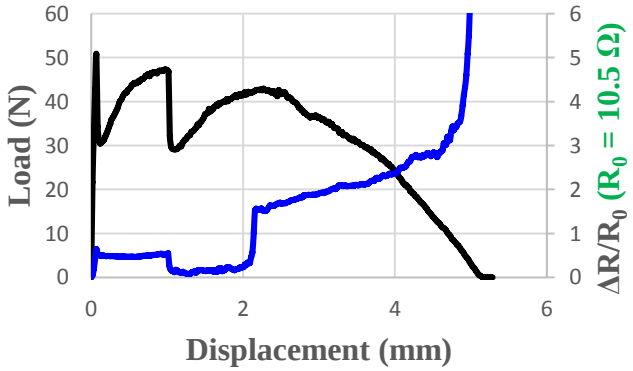

Fig. 8. Mode I results of CFRP laminate coupon with debonding from two electrodes; black line indicating bridging force; blue line showing fractional TTER change.

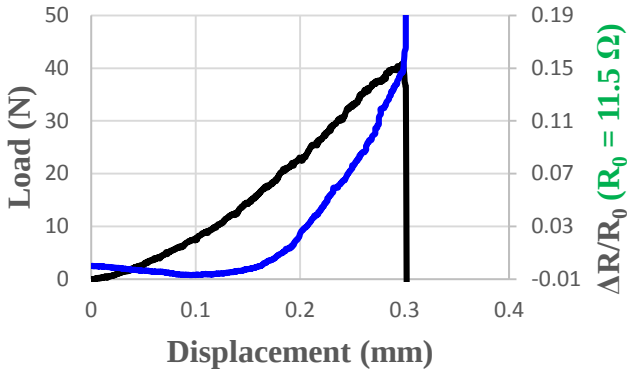

Fig. 9. Mode II results of single Z-pin reinforced CFRP laminate; black line indicating bridging force; blue line showing fractional TTER change.

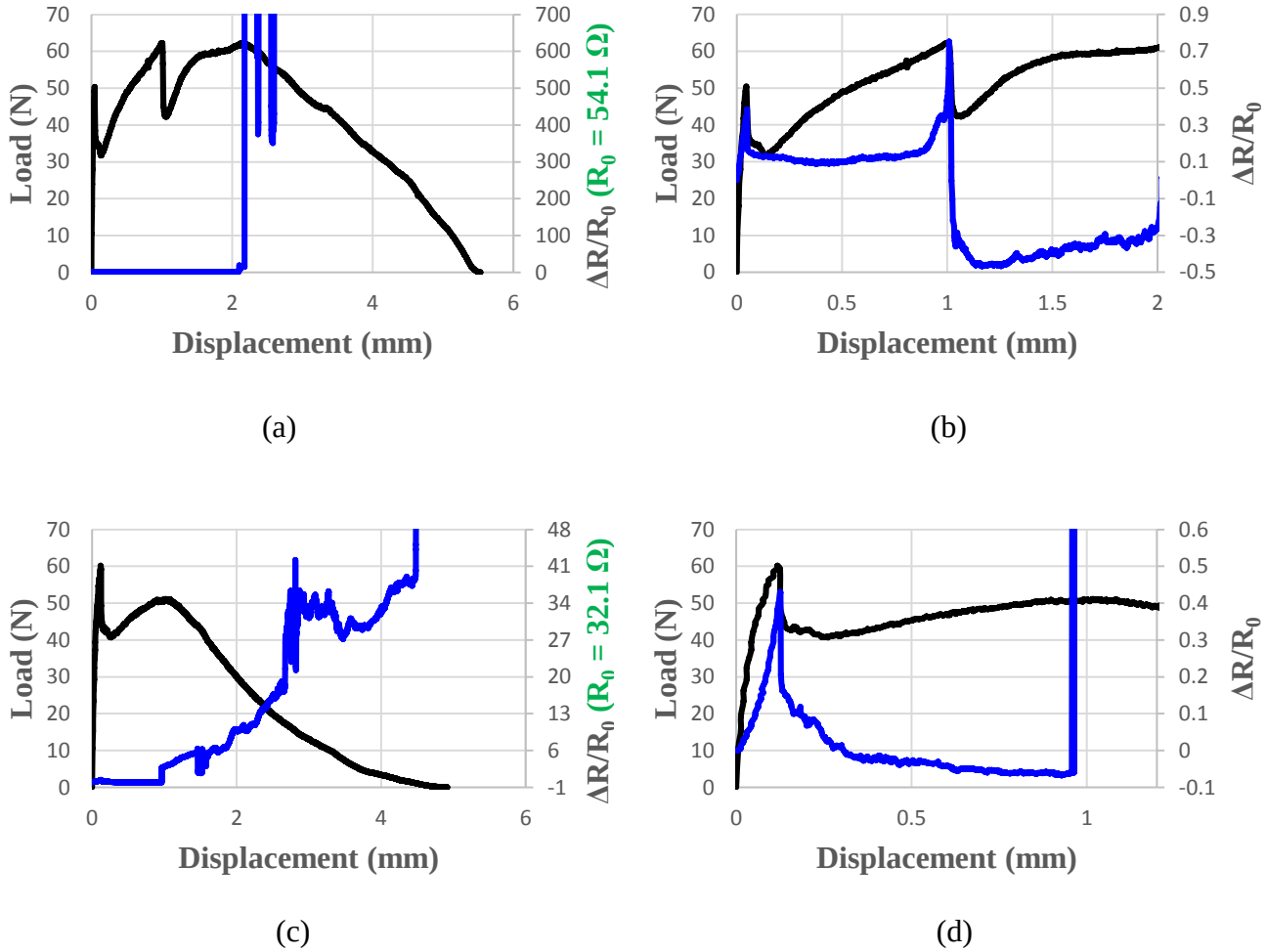

Fig. 10. Mode I results of single Z-pin reinforced GFRP laminates; (a) full-range and (b) partially enlarged plots of the coupon without sensing in stage III; (c) full-range and (d) partially enlarged plots of the coupon with sensing in stage III; black lines indicating bridging forces; blue lines showing fractional TTER changes.

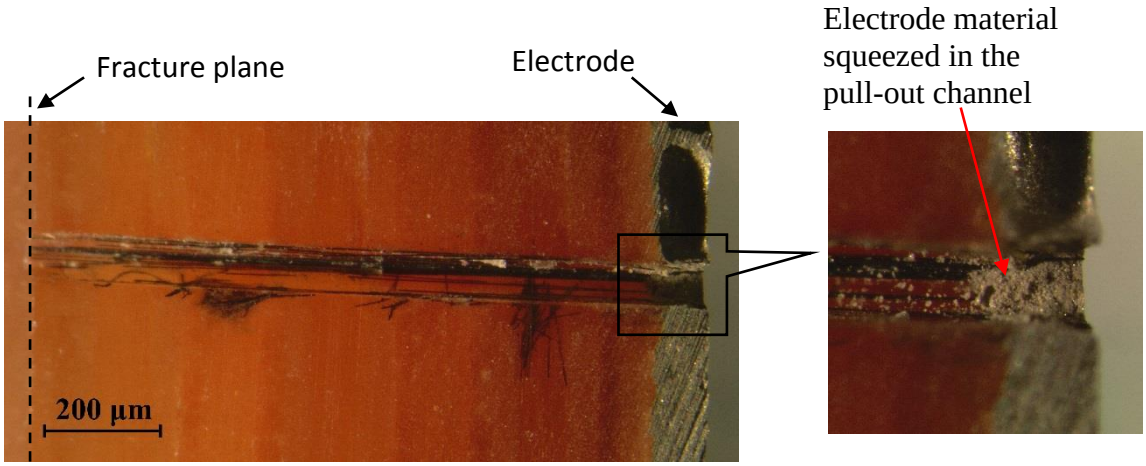

Fig. 11. Micrograph of the pull-out channel with residual Z-pin fibres.

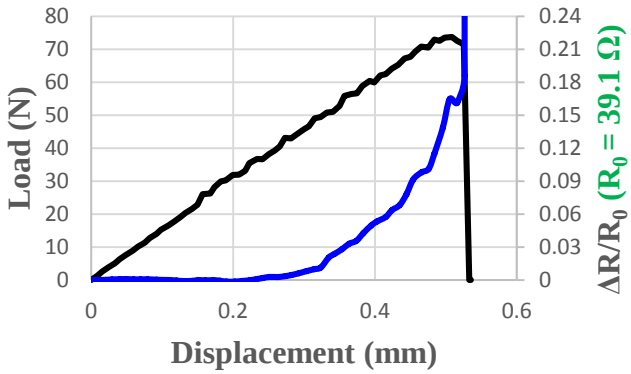

Fig. 12. Mode II results of single Z-pin reinforced GFRP laminate; black line indicating bridging force; blue line showing fractional TTER change.